Journal of Polymer Research (2023) 30:294
https://doi.org/10.1007/s10965-023-03672-z

ORIGINAL PAPER

Electrospun nanocomposite membranes for wastewater treatment: γ-alumina nanoparticle incorporated polyvinyl chloride/thermoplastic polyurethane/polycarbonate membranes

Javad Yekrang[1] · **Habib Etemadi**[2]

Received: 30 January 2023 / Accepted: 27 June 2023 / Published online: 6 July 2023

Abstract
In this study, the nanocomposite membranes were electrospun using conventional polymers, including polyvinyl chloride (PVC), thermoplastic polyurethane (TPU) and polycarbonate (PC) at different levels of incorporation of the γ-alumina nanoparticles (1, 3 and 5 wt.%). Morphological investigation using SEM images showed that the diameters of the nanofibers were in the range of 155-491 nm. The energy dispersive spectroscopy (EDS) analysis and FTIR test revealed the presence of the γ-alumina nanoparticles (NPs) and characteristic chemical groups in electrospun nanocomposite membranes (ENCMs). The contact angle test showed that the hydrophilic features of the membranes improved with the incorporation of γ-alumina NPs with the decrease of contact angle from 80° to 27°. Mechanical tests exhibited a drop in tensile strength and strain of the nanocomposite membranes by adding more γ-alumina NPs to the neat membrane. Filtration efficiency of ENCMs was evaluated using the submerged system with the humic acid (HA) solution. Results showed that the permeation flux of the membranes increased with an increase in the content of the γ-alumina NPs (from 49 to 102 $L.m^{-2}.h^{-1}$). The irreversible fouling ratio (IFR) of the membranes was also improved by increase in the content of the γ-alumina NPs up to 3 wt.%. Results also demonstrated the better anti-fouling performance for the blended nanofiber membrane with 3 wt.% of the nanoparticles (flux recovery ratio, FRR=94.4 %). HA rejection test also proved the enhanced foulant removal (99.6 %) of ENCM containing 3 wt.% γ-alumina NPs.

Keywords Water treatment · Nanocomposite · Nanofiber membrane · γ-alumina nanoparticles · Anti-fouling

Introduction

Drought stress and water availability have become a major concern worldwide which have affected multiple aspects of humankind's life, economic sectors, environmental systems and agricultural production, especially in the case of countries of North Africa and the Middle East [1, 2]. Water resources are in a challenging situation globally caused by several factors, such as economic development, population growth, climate change, etc. Recycling and reuse of wastewater have presented potential opportunities towards producing new sources of potable water [3, 4].

The most current technologies that are involved with water purification are chemical [5–7], physicochemical [8, 9] , biological [10, 11] and combined treatments [12, 13]. The membrane-based technologies (as a physicochemical method) have also attracted great attention for wastewater purification due to advantages such as selective treatment, high separation efficiency, stability, higher permeation flux, low energy consumption, cost-effectiveness and eco-friendly aspects [14]. The electrospun nanofibers have been extensively applied in different fields, including health care, energy devices, biomedical and environmental applications due to their high surface-to-volume ratio, ability of functionalization and interconnected pores [15]. The nanofibrous membranes have also introduced new opportunities for wastewater treatment due to their high flux and lower energy consumption than conventional membranes [16–18]. The most common polymers for the electrospinning

✉ Javad Yekrang
j.yekrang@ubonab.ac.ir

[1] Department of Textile Engineering, University of Bonab, Bonab 5551395133, Iran

[2] Department of Polymer Science and Engineering, University of Bonab, Bonab 5551395133, Iran

of water filter media are polyacrylonitrile (PAN) [19–21], polycarbonate (PC) [22], polyvinyl chloride (PVC) [23, 24], polystyrene (PS) [25], polyurethane (PU) [26, 27], polyvinylidene fluoride (PVDF) [28, 29] and polyether sulfone (PES) [30]. Polyvinyl chloride and polycarbonate polymers exhibit many advantages, including optimal tensile strength, wear resistance, stability against chemicals and being economically viable, which make them suitable for water treatment applications. However, PVC and PC have some limitations, such as low hydrophilicity and high brittleness [31, 32]. Thermoplastic polyurethane exhibits superior mechanical properties, which makes it a good candidate for enhancement of the strength and extensibility of membranes [33]. Considering the pros and cons of different polymers, polymer blending is applied to improve essential properties of membranes, including the hydrophilicity, anti-fouling feature, water flux and filtration efficiency [9, 34–37]. However, most of the researches have focused on the air filtration capability of PVC, PC and TPU nanofiber membranes [22, 38, 39]. The lack of studies could be attributed to the disadvantages of these polymers, regarding low hydrophilicity and the poor anti-fouling properties. In our previous work, we electrospun blended membranes of PVC/PC/TPU to investigate their capability for wastewater treatment [33]. Results showed that the electrospun nanofiber membranes exhibited good performance in rejecting the organic pollutant from the contaminated water. However, the hydrophilicity of the membranes remained a challenging issue.

Functionalization by multifunctional hydrophilic materials and nanoparticles could be used as an efficient way to enhance the hydrophilic property and filtration performance of the electrospun nanofiber membranes (ENMs) [40]. The most used method for the functionalization of nanofiber membranes is thee incorporation of the carbon nanomaterials, metal nanoparticles and inorganic materials in electrospinning solution [41]. Different nanoparticles have been used to modify the characteristics of ENMs, including titanium dioxide (TiO_2) [42, 43], zinc oxide (ZnO) [20, 44, 45] and silver (Ag) NPs [46, 47]. Aluminum oxide (alumina, Al_2O_3) NPs widely used as an enhancer for the hydrophilic properties of water purification membranes [48–50]. Alumina oxide NPs are low-cost and highly stable particles with excellent surface chemistry features. The terminal hydroxyl groups on the alumina could also enhance the hydrophilicity and improve the anti-fouling quality of the membranes [51]. However, there is no study to evaluate the influence of alumina NPs in filtration performance and fouling of blended ENMs.

In this paper, we attempted to electrospun PVC/TPU/PC membranes incorporated with three concentrations of the γ-alumina NPs (1, 3 and 5 wt.%). We also studied the effect of the content of the γ-alumina NPs on the morphological properties, wettability, chemical structure, tensile strength, water filtration performance and anti-fouling features of ENCMs. Thermoplastic polyurethane was employed to increase the elasticity and mechanical strength of ENCMs membranes. Polycarbonate and polyvinylchloride polymers also were used due the economic issues in the manufacturing of membranes. Furthermore, the solubility parameter (δ) of the selected polymers was similar to each other (PVC=21.9, PC=19.5 and TPU= 20 [$MPa^{1/2}$]) [52–54], which facilitates their miscibility in the blended matrix. The nanofibrous structure was also used for its high porosity and specific surface area and interconnectivity of the pores, which could enhance the water flux and improve the fouling properties of the electrospun membranes compared to traditional microfiltration (MF) membranes, which is desirable in pressure-driven separation [55, 56]. It was also believed that the incorporating of the γ-alumina NPs into blended PVC/TPU/PC nanofibers could improve the hydrophilicity, fouling behavior and water filtration efficiency of ENCMs.

Materials and methods

Martials

Polyvinyl chloride (M_w = 80,000), polycarbonate and Cetyltrimethylammonium bromide (CTAB) were supplied from Sigma Aldrich Co., USA. TPU (Desmopan 588E) was purchased from Bayer Co., Ltd., Germany. Tetrahydrofuran (THF, 99%) and N, N-dimethylformamide (DMF, 99%) solvents were received from Merck Co, USA. The aluminum oxide nanoparticles (γ-Al_2O_3, 99.9%, 20 nm) were purchased from SkySpring Nanomaterials, Inc., USA. Humic acid (HA, Sigma Aldrich Co., USA) was used to examine the filtration performance and pollutant rejection of ENCMs. Sodium hydroxide (NaOH, ≥ 98%) and hydrochloric acid (HCl, 37%) were also provided by Merck Co., USA. HCl and NaOH were used to adjust the pH of the humic acid solutions.

Preparation of the electrospinning solutions

1 g of the polyvinyl chloride powder and 1 g of TPU pellets were independently dissolved in 10 g of THF/DMF 50:50 v/v% solvents to prepare 10 w/w% PVC and TPU solutions, respectively. The prepared solutions were then stirred for 4 h at ambient temperature. The γ-alumina NPs were added to 10 g of THF/DMF 70:30 v/v% solvent, and the suspension was sonicated for 15 min at a frequency of 25 Hz for dispersion to prevent aggregation of the γ-alumina NPs. Then, 1.6 g of polycarbonate powder was added to the γ-alumina loaded solvent and stirred for 2 h at ambient temperature to prepare the 16 w/w% PC solution. CTAB surfactant (0.2 w/w/%) was added to the PC solution to facilitate the

electrospinning of the solution. The γ-alumina NPs were added to the solvents, so that three different percentages of nanoparticles were obtained in the PC solutions (1, 3 and 5 wt.%). The prepared solutions of PVC, PC and TPU were then mixed at PVC:TPU:PC ratio of 25:25:50. The blended solution was stirred for 1 h at ambient temperature. A control sample was also electrospun without the addition of γ-alumina NPs to compare with ENCMs.

Electrospinning of ENCMs

The schematic of the solution preparation and the electrospinning procedure is presented in Fig. 1. The blended solution containing γ-alumina NPs was electrospun using a syringe needle within an electrostatic field (18 kV) at 0.6 mL/h flow rate. The nanofiber membranes were electrospun randomly on a reciprocating rotating drum (250 rpm) covered by aluminum foil. The distance between the needle tip (gauge 23) and the collector drum was adjusted at 20 cm. The electrospinning was performed for 300 min to produce sufficient thickness of ENCMs.

Characterization of the membranes

Morphology of the electrospun membranes

The morphological features of ENCMs were evaluated using scanning electron microscopy (SEM) images. The MIRA3 XMU microscope was used to capture SEM images of the platin sputtered ENCMs (at 5000X magnification). Digimizer (version 6.1.1) software was also applied to measure the diameter of the nanofibers at 100 random places in SEM images. The energy dispersive X-ray spectroscopy (EDS) analysis was also used for identifying and quantifying the elemental composition of ENCMs.

FTIR analysis

FTIR spectroscope (Shimadzu 8600S, Japan) was used to study the absorption peaks of the functional groups in the membranes loaded by γ-alumina NPs. Thin pellets were made by mixing the tiny pieces of samples and potassium bromide (KBr) powder. The prepared pellets were used to record FTIR spectrum of ENCMs in the region of 500-4000 cm^{-1}.

Hydrophilicity and porosity of ENCMs

The water contact angle (WCA) of ENCMs was measured to evaluate the hydrophilicity of the γ-alumina loaded membranes. Jikan CAG-10 (Jikan Co., Iran) was used to drip a water drop on the surface of ENCMs. The image of the water drop was obtained 9 s after the drop came into contact with the surface of the nanofiber webs. Three tests were conducted on the surface of ENCMs, and the average values of WCA were calculated. ImageJ 1.53n software was employed to measure WCA of the electrospun membranes.

The gravimetric technique was used to measure the porosity (ε) of the γ-alumina NPs incorporated membranes using Eq. (1) [50]:

$$\varepsilon\,(\%) = \frac{\left(m_w - m_d\right)/\rho_w}{\left(m_w - m_d\right)/\rho_w + m_d/\rho_p} \times 100 \tag{1}$$

where m_d (g) and m_w (g) are the weights of dry (at 65 °C for 6 h) and wet membranes (for 24 h in water), respectively.

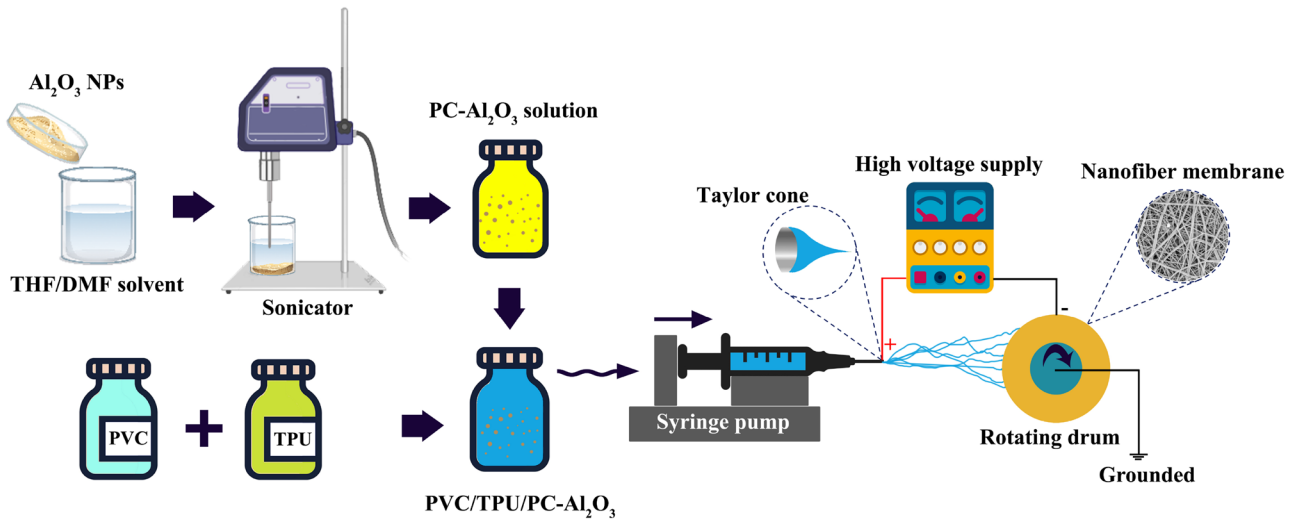

Fig. 1 The electrospinning schematic of ENCMs loaded by γ-alumina NPs

ρ_w and ρ_p also represent the density of water (0.998 g.cm^{-3}) and the blended matrix, respectively. The general rule of mixtures was used to calculate the density of the blended membranes. Considering the density of TPU (1.24 g.cm^{-3}), PC (1.20 g.cm^{-3}), PVC (1.38 g.cm^{-3}) and γ-alumina NPs (3.95 g.cm^{-3}), the ρ_p was calculated as 1.26, 1.33, 1.38 and 1.43 g.cm^{-3} for membranes containing 0, 1, 3 and 5 wt.% of γ-Al_2O_3, respectively.

Mechanical experiments

ASTM D882 method was used to measure the stress and strain at the rupture of ENCMs. The Zwick universal machine (ZwickRoell Co., Germany) was applied to determine the mechanical properties of ENCMs (rectangular shaped, 60 mm × 10 mm). The gauge length and test speed were set at 30 mm and 10 mm/min, respectively [50]. Five experiments were carried out on each membrane, and the average values were reported.

Flux test

The laboratory testing setup was employed to examine the anti-fouling features and contaminant rejection of ENCMs. Figure 2 demonstrates the schematic of the filtration unit. The test specimen was fixed on the submerged module with an (A = 14.7 cm^2) and a diffuser was used to create air turbulence in the test solution at the rate of 4 L.min^{-1}. The air flow was used to create a homogenous solution of the humic acid and to prevent from deposition of the foulants on the surface of ENCM. The humic acid solution (1 g.L^{-1}) was used as contaminated water model (pH 7). The flux of the pure water (F_{W1}) of ENCMs was measured before the flux test with the polluted water. The pure water test was performed for 30 min at 0.8 bar vacuum pressure to minimize the compactness effect of ENCMs. Equation (3) was used to calculate the flux of the pure water at the steady state condition [50]:

$$F_{W1} = \frac{V}{A \times t} \tag{3}$$

where V (L) is the volume of the permeated water and A (m^2) and t (h) are the effective surface area of ENCMs and the test time, respectively.

HA rejection test was carried out after the pure water flux experiment. The test was conducted using water/HA solution at a vacuum trans-membrane pressure (TMP) of 0.2 bar. The experiment was conducted for 240 min at intervals of 15 min. The flux of the humic acid solution (F_{HA}, L.m^2.h^{-1}) was measured by collecting and weighting the permeated water. The membrane was then removed, and the filtration cake

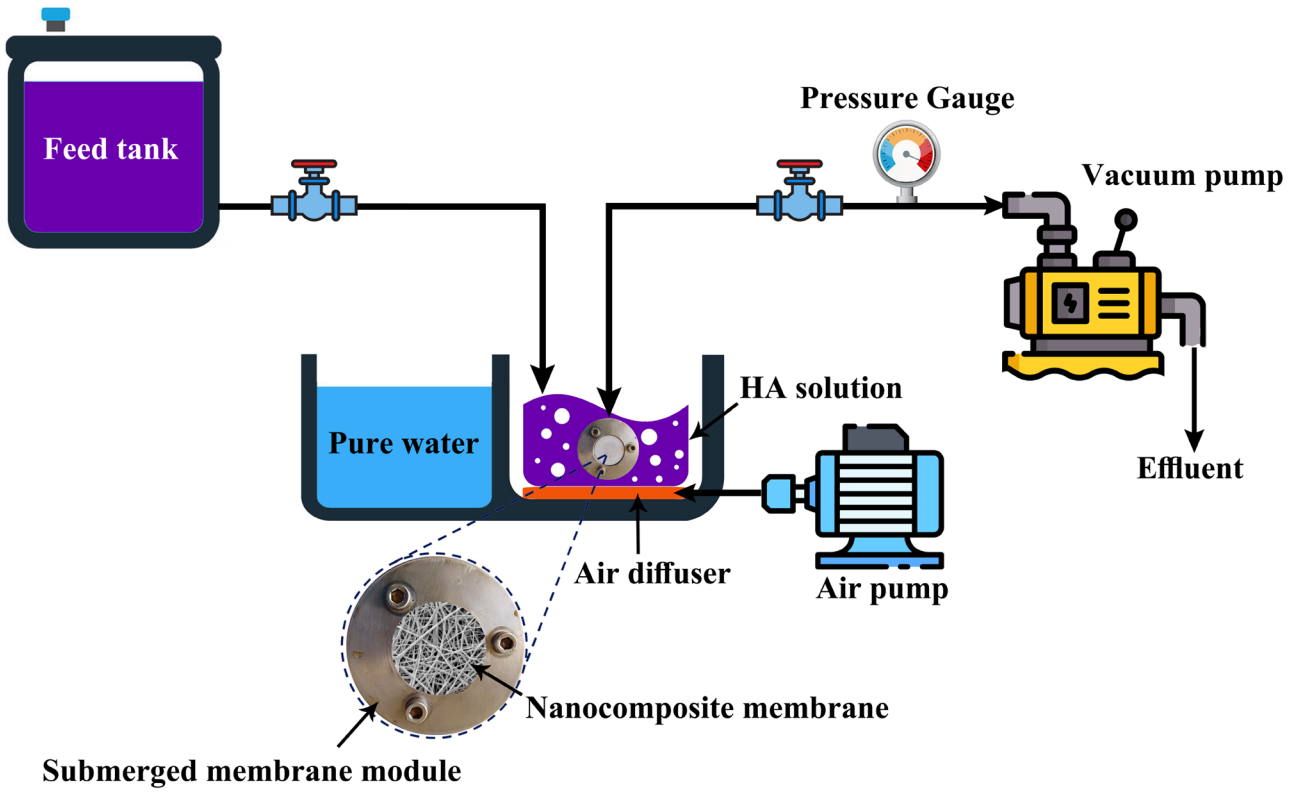

Fig. 2 The schematic of the flux testing setup for evaluation of the filtration efficiency of ENCMs

was cleaned gently with the distilled water. The membrane then reassembled in the submerged module in the pure water tank. The flux of the pure water after the fouling test (F_{W2}) was also measured using Eq. (3). The flux recovery ratio (*FRR*) of ENCMs was calculated using Eq. (4) [50]:

$$FRR\,(\%) = \left(\frac{F_{W2}}{F_{W1}}\right) \times 100 \tag{4}$$

The irreversible fouling ratio (*IFR*), reversible fouling ratio (*RFR*) and total fouling ratio (*TFR*) of ENCMs were obtained using Equations (5) to (7) [50]:

$$RFR\,(\%) = \left(\frac{F_{W2} - F_{HA}}{F_{W1}}\right) \times 100 \tag{5}$$

$$IFR\,(\%) = \left(\frac{F_{W1} - F_{W2}}{F_{W1}}\right) \times 100 \tag{6}$$

$$TFR\,(\%) = RFR + IFR = \left(\frac{F_{W1} - F_{HA}}{F_{W1}}\right) \times 100 \tag{7}$$

Equation (8) was used to calculate the rejection rate of the pollutant (*R*, %) as a representative of the efficiency of the foulant rejection of ENCMs [50]:

$$R(\%) = \left(1 - \frac{C_P}{C_f}\right) \times 100 \tag{8}$$

where C_f and C_p are the concentration of the pollutant ($g.L^{-1}$) in the fed and permeated water, respectively. The ultraviolet spectrometer (Shimadzu UV-1800, Japan) was used to determine the concentration of the humic acid in the permeated solute at 250 nm wavelength.

Results and discussion

Morphological investigation of ENCMs

The morphological properties of ENCMs were investigated using SEM images. Figure 3 shows the SEM images of the neat membrane (NFM) and ENCMs containing 1, 3 and 5 wt.% of the γ-alumina NPs. Minitab 21.1.0 software was applied to plot the diameter distribution histogram of ENCMs. SEM images revealed that the nanofiber structures had been successfully electrospun at different contents of the γ-alumina NPs. As can be seen, the agglomeration of the γ-alumina nanoparticles occurred at a few places of the longitudinal direction of the nanofibers at 1 and 3 wt.% of the nanoparticle contents (see Fig. 3b, c). The aggregation of the γ-alumina NPs depends on the dispersion step before preparation of the polymer solutions. The γ-alumina NPs were dispersed within the solvent system of the PC solution using the ultrasonic method. Sonication is an effective method to prevent from agglomeration of NPs [57]. The effectiveness of the sonication process to prevent agglomeration could be enhanced by the simultaneous use of surfactant agents and pH adjustment of the solution [58–60]. However, adding any chemical agents (such as surfactants) or changing the pH of the solution will change the electrospinning stability, surface tension of the polymer jet, and formation of the nanofibers [61]. Consequently, the preparation of entirely uniform nanofibers without aggregation of the nanoparticles cannot be expected, and the outcome of the sonication process is uncertain [61–63]. Moreover, agglomerations often occur at high particle concentrations (in blend electrospinning) [64]. The time and frequency of the sonication process can also affect the dispersion of the nanoparticles within the solution [65, 66]. Furthermore, the concentration and viscosity of the polymer matrix can affect the way the particles aggregate. The γ-alumina nanoparticles were mixed and stirred mechanically two steps after the sonication process, firstly in a concentrated solution (PC, 16 wt.%) and the second step in the polymer mixture. The two stages of the mechanical stirring and higher viscosity of the polymer solution could also be responsible for the re-agglomerating some of the nanoparticles within the polymer matrix.

Figure 3d represents the microscopic image of the electrospun membrane loaded with 5 wt.% of the γ-alumina NPs. It seems that the formation of the nanofiber structures is disrupted with the increase in the content of the nanoparticles to 5 wt.%. The increase in the content of the γ-alumina NPs leads to a significant raise in the conductivity of the electrospinning solution. The stretching of the polymer jet in the electrostatic field would be increased with an increase in the conductivity of the solution. As a result, there is less time for the solvent to escape, and the polymer spreads over the collector before the fiber-like structure is formed. It is also evident that the bead-like points had been created with the increase in the content of the nanoparticles to 5 wt.%. The average, standard deviation and the coefficient of variation (CV%) of the diameters of ENCMs are listed in Table 1.

Results showed a decrease in the nanofiber diameters from 323 nm to 263 nm with the increase in the content of the γ-alumina NPs from 1 to 5 wt.%. The solution conductivity is increased with the increase in the content of the aluminum oxide NPs. Solution conductivity is an effective parameter that can affect the electrospinning process. The charge density of the polymer solution increases with the increase in solution conductivity, which is resulted in more stretching forces within the electrostatic field, and the creation of the finer nanofibers [67]. It was also found that the

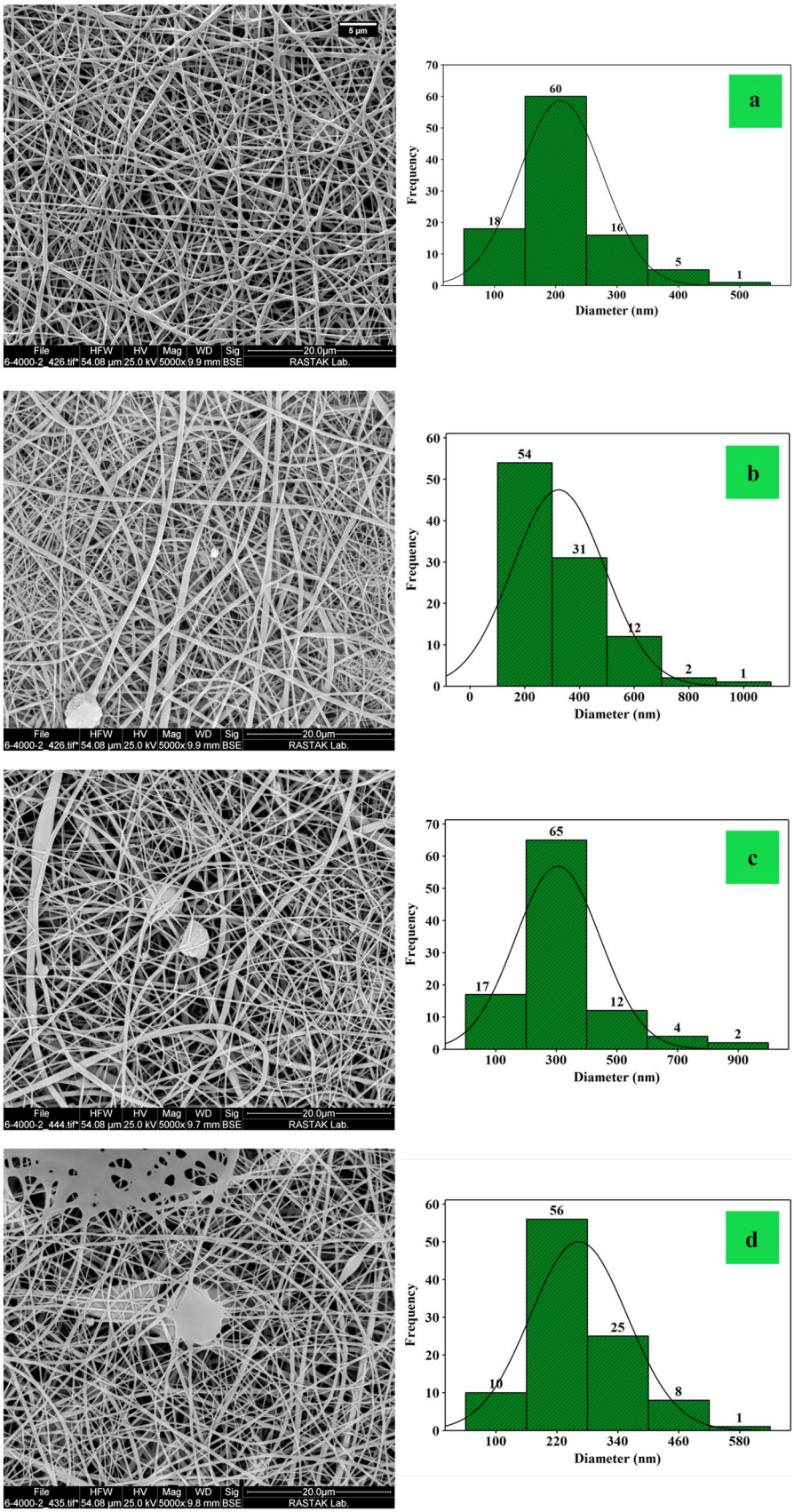

Fig. 3 SEM images of ENCMs at different content of the γ-alumina NPs: (**a**). 0 wt.% (**b**). 1 wt.%, (**c**). 3 wt.%, (**d**). 5 wt.%

Table 1 The results of diameter measurement of the nanofiber membranes using SEM images

Membrane	Morphology of the nanofibers	Diameter (nm)	CV%
NFM	No beads-nanofiber formation	208 ± 67	32
NFM-Al 1 wt.%	No beads-agglomeration of NPS	323 ± 168	52
NFM-Al 3 wt.%	No beads-agglomeration of NPS	304 ± 104	34
NFM-Al 5 wt.%	Bead formation- polymer spread	263 ± 95	36

average diameter of ENCMs was increased with the addition of the γ-alumina NPs. The nanofiber diameters were increased from 208 nm to 323 nm at 1 wt.% of the γ-alumina NPs. The nanoparticles are surrounded by the polymer matrix to form the nanofiber structures. The addition of the nanoparticles to nanofiber membranes leads to the covering of the more nanoparticles by polymer solution, resulting in to increase in the diameter of the nanofibers compared with the neat PVC/TPU/PC nanofibers. It is also concluded that the addition of the γ-alumina NPs had led to a decrease in the uniformity of the nanofibers. CV% of the diameter of the nanofibers was increased from 32% in the neat membranes to 52, 34 and 36% in ENCMs containing 1, 3 and 5 wt.% of the γ-alumina NPs, respectively. This result can be assigned to the agglomeration of the nanoparticles within the polymer matrix of the nanofibers. The nanoparticles were agglomerated in different sections of the longitudinal direction of the nanofibers surrounded by PVC/TPU/PC blended polymer matrix. Thus, the variation of the diameter of the nanofibers would be increased in the γ-alumina NPs incorporated membranes [64].

Minitab software was used to conduct the one-way analysis of variance (ANOVA) at a 95% confidence level ($\alpha = 0.05$) to analyze the effect of the addition of the γ-alumina NPs on the diameter of ENCMs. The ANOVA analysis showed that the content of the γ-alumina NPs had a significant impact on the diameter of ENCMs (p-value = 0.007 < 0.05).

EDS results

The energy dispersive spectroscopy (EDS) spectrums of the alumina-loaded ENCM and EDS-SEM images of the data

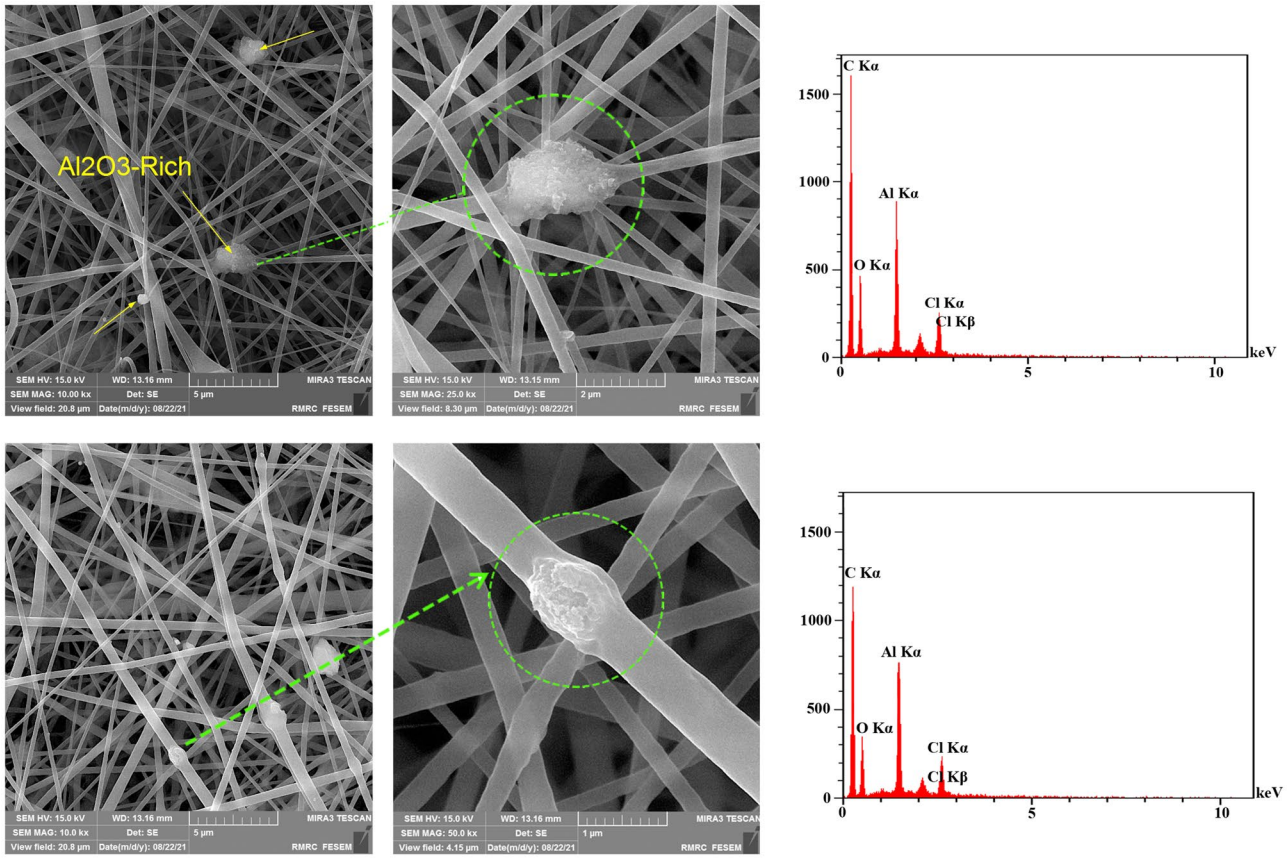

Fig. 4 SEM-EDS images and energy dispersive spectrum of the electrospun nanofiber membrane loaded by γ-alumina NPs (NFM-Al 3 wt.%)

Table 2 The elemental composition in the (PVC/TPU/PC)-Al_2O_3 nanofiber membrane (NFM-Al 3 wt.%)

Element	Line	Int	K	Kr	wt.%
C	Kα	416.8	0.7517	0.3056	67.43
O	Kα	128.8	0.1157	0.0470	25.47
Al	Kα	278.0	0.0875	0.0356	4.87
Cl	Kα	96.4	0.0451	0.0183	2.23

collection area, are illustrated in Fig. 4. The percentage of each element is also given in Table 2. The energy dispersive spectroscopy test was only performed on the ENCM containing 3wt.% of the γ-alumina NPs to evaluate the elemental composition of ENCMs. The EDS results confirmed the presence of all elements of the involved materials (see Table 2). The peak of Al and O elements originate from the γ-alumina (Al_2O_3) NPs. The presence of O element can also be attributed to polycarbonate (C_5 H_{16} O_2) and TPU polymers. The observed peak for the Cl element can be assigned to the elemental composition of PVC (C_2H_3Cl) polymer. The EDS results revealed the presence of the γ-alumina NPs in the electrospun nanofiber membranes. EDS-SEM images in Fig. 4 also demonstrated clustered spots rich in nanoparticles.

FTIR results

FTIR technique was used to investigate the presence of the functional groups and chemical bonds in ENCMs. Figure 5 demonstrates FTIR spectra of ENCMs at different contents of the γ-alumina NPs. The absorbance peak near 3000 cm^{-1} represented the presence of C-H bonds in CH_2 and methyl groups (CH_3) of TPU [68]. The characteristic peak at 3330 cm^{-1} correspond to N-H functional groups. The intense peaks at 1220, 1720 and 1770 cm^{-1} could be attributed to C-H bonds and C-N stretching of carbonyl groups, respectively [68]. The observed peaks at 1160 and 1080 cm^{-1} could be responsible for C-O-C stretching.

The absorption peak at 714 cm^{-1} in the PVC spectrum could be related to C-C stretching. The peaks at 1226 cm^{-1} and 1450 cm^{-1} could be responsible for C-H rocking and CH_2 deformation, respectively. The absorption peak in the region of 2900 to 2970 cm^{-1} could be attributed to C-H stretching [32]. The fingerprint peaks of PC at 1230 and 1080 cm^{-1} correspond to the stretching of the C-O bond. The intense peaks at 1770 and 1220 cm^{-1} were related to C=O bonds [69]. The absorption peaks at 1400 and 1450 cm^{-1} could be explained by the bending vibration of C-H bonds and C=C stretching, respectively.

The FTIR spectrum of the NFM sample (0 wt.%) shows all the abovementioned characteristic peaks for the PC, PVC and TPU polymers. There is an elementary peak near 3330 cm^{-1}, which could be assigned to N-H stretching, indicating the presence of the functional groups of the polyurethane in the matrix. The IR spectra of the blended membrane thus showed no chemical interaction between the constituent polymers.

The FTIR results for γ-alumina incorporated ENCMs also demonstrated that the elementary peaks of the PVC/TPU/PC membrane remained unchanged. Accordingly, the broad absorption peak between 3100-3500 cm^{-1} could be corresponded to the overlap of OH stretching vibrations of the adsorbed water molecules by the γ-alumina NPs and N-H stretching in the blended membrane [70]. The intense peaks between 700 and 900 cm^{-1} correspond to the O-Al-O vibrations. The peaks near 600-700 cm^{-1} could also be ascribed to Al-O bending and stretching vibrations [71]. FTIR results confirmed the presence of the γ-alumina NPs and functional groups of PC, PVC and TPU polymers in nanocomposite structures without any other chemical reaction.

Hydrophilic properties and porosity of ENCMs

The total porosity of the neat and nanocomposite nanofiber membranes was measured using Eq. (1). Table 3 shows the density and porosity of ENCMs. The total porosity of ENCMs was increased significantly (p-value = 0.006 < 0.005) by adding the γ-alumina NPs in nanofiber membranes from 70% to 86%. It has been reported that modifying the phase inversion membranes by γ-alumina NPs improved the porosity features [49]. The γ-alumina NPs (as the high hydrophilic agents) absorb more water during immersion in the water environment, resulting in to increase in the hydroxyl content of the membranes [72]. Thus, the incorporation of the γ-alumina NPs leads to an increase in the total porosity of the nanocomposite membranes. Consequently, the total porosity of ENCMs increased from 86.4% to 90.3% with more increase in the content of the γ-alumina NPs.

Figure 6 shows the results of the contact angle test of ENCMs. WCA was measured to investigate the hydrophilic properties of ENCMs (see Table 3). The results indicated that the incorporation of the γ-alumina NPs in the nanofiber membranes has reduced the WCA of ENCMs, resulting from improving hydrophilicity of ENCMs. WCA decreased from 80.3° (for nanofiber membrane) to 73.4° by embedding 1 wt.% of the γ-alumina NPs. It was also observed that the further incorporation of the γ-alumina NPs led to significant improvement in the hydrophilic features of ENCMs. The contact angle of the nanocomposite membranes decreased from 73.4° to about 27° with the increase in the content of the γ-alumina NPs from 1 to 5 wt.%. Figure 6d to f represent the hydrophilic behavior of NFM-Al 5 wt.% membrane at different frames (time intervals of 3 s). As can be seen, the water droplet spread gradually over the surface of NFM-Al 5 wt.% membrane during the test time (9 s) and remained unchanged at the contact angle of about 27° (see

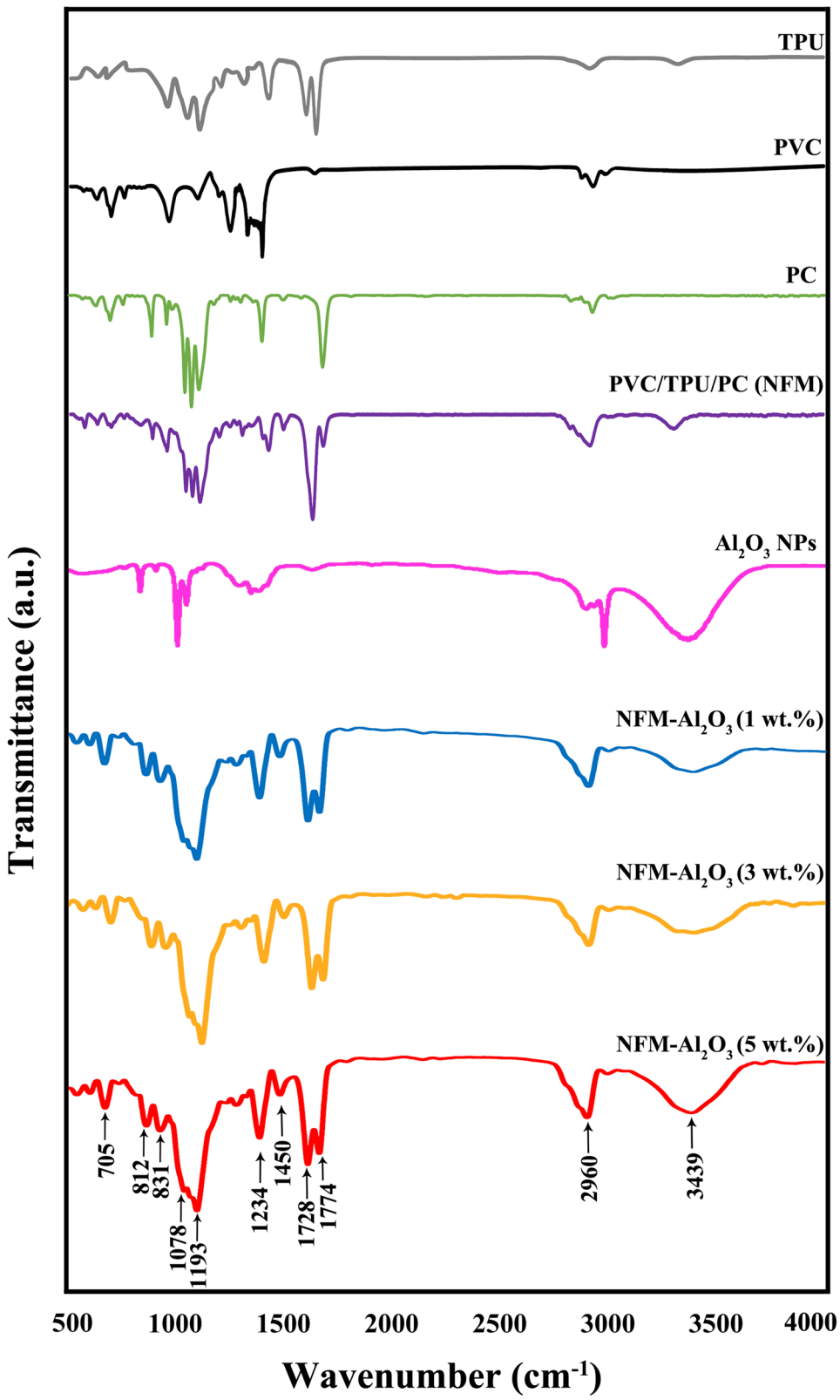

Fig. 5 FTIR spectrum of the neat PC, TPU, PVC, γ-alumina NPs and ENCMs at different contents of the γ-alumina NPs (0, 1, 3 and 5 wt.%)

Fig. 6d to f). The nanocomposite membrane, thus exhibited super-hydrophilic properties with the incorporation of the higher levels of the γ-alumina NPs. The enhancement in the hydrophilicity of ENCMs could be explained by the excellent hydrophilic characteristics of the alumina nanoparticles [50, 73].

Table 3 Density, porosity and water contact angle of ENCMs

Membrane	Density ($g.cm^{-3}$)	Total porosity (%)	Contact angle (degree)
NFM	1.26	70.2 ± 3.9	80.3 ± 0.8
NFM-Al 1 wt.%	1.33	86.4 ± 5.4	73.4 ± 2.6
NFM-Al 3 wt.%	1.38	88.7 ± 4.7	62.8 ± 2.1
NFM-Al 5 wt.%	1.43	90.3 ± 3.1	27.3 ± 1.5

The primary organic pollutants in the water are hydrophobic [74]. These hydrophobic matters have more affinity to attach to the membrane surface due to hydrophobic interactions. Moreover, the hydrophilicity of ENCMs enhances the formation of a layer of water on the membrane surface, which can limit the pollutant adsorption or deposition on the surface [73, 75]. The hydrophilic modification is known as an anti-fouling strategy for MF membranes [76, 77]. Wang et al. developed the super-hydrophilic polyphenylsulfone (PPSU) nanofiber membranes by plasma treatment [78]. They reported that the plasma treatment could enhance the water contact angle of PPSU membranes from 137° to 0°, making it a candidate to use as a support layer for thin-film composite membranes. Literature also reported the improvement in fouling behavior of the super-hydrophilic nanofiber membranes, especially for oil/water separation: (PANI/PAN, WCA < 5°) [79] and (PVDF/PAN, WCA = 0°) [80]. Moreover, improving the fouling performance of the nanofiber membranes has been reported for hydrophilic modifications by embedding of the nanoparticles such as ZnO (decrease in WCA from 80° to 55.5°) [81] and graphene oxide (decrease in WCA from 87° to 0°) [82]. Accordingly, it was expected that the enhancement in the hydrophilic features of the γ-alumina NPs incorporated ENCMs could improve the anti-fouling characteristic of the membranes. ANOVA analysis also confirmed that the content of the γ-alumina NPs had a significant effect (p-value=0.000 <0.005) on the hydrophilic properties of ENCMs.

Mechanical properties of ENCMs

Figure 7 demonstrates the stress-strain curves and the measured values of the tensile strength and strain at the rupture of ENCMs. The results indicated that the incorporating the γ-alumina NPs in the electrospun membranes has caused a drop in mechanical and elastic properties. The stress and strain at break of the nanofiber membranes were decreased from 3.5 to 2.81 MPa (about 20% decrease) and 40.60 to 29.30% (a drop of about 28%) by adding 1 wt.% of the γ-alumina NPs to the neat nanofiber membranes, respectively (see Fig. 7b, c). The further incorporation of the γ-alumina NPs in the nanocomposite membranes led to a dramatic drop in the mechanical properties of the membranes. The stress and strain at the rupture of ENCMs were

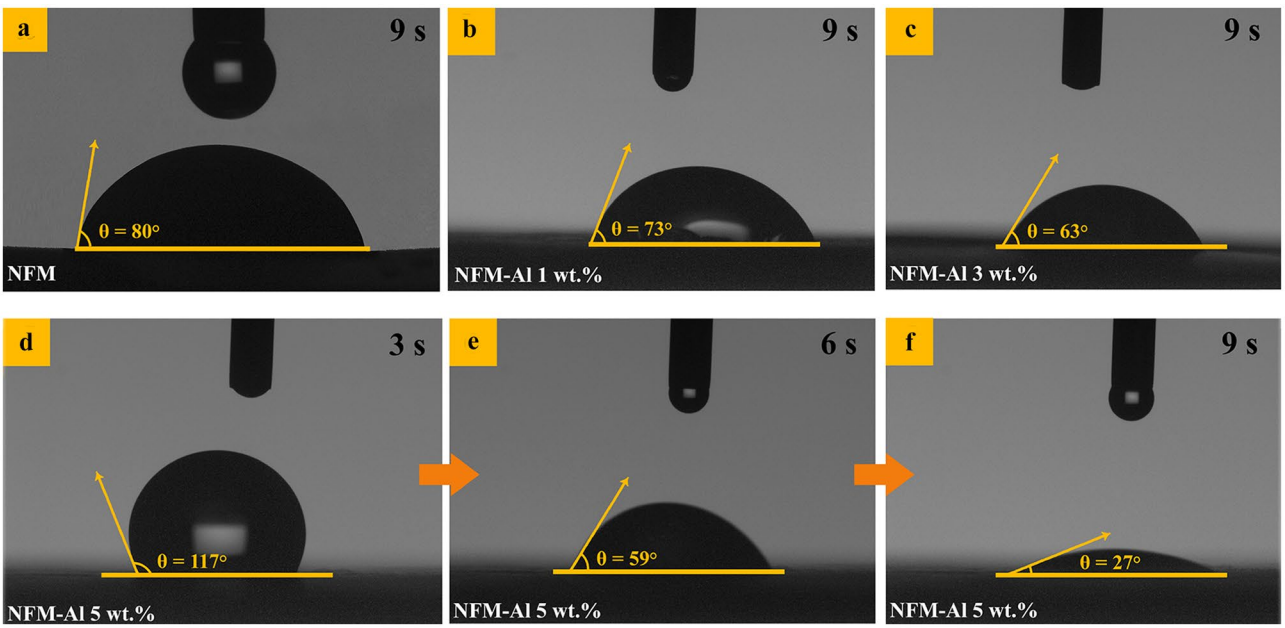

Fig. 6 The water contact angle of ENCMs (**a**). neat PVC/TPU/PC (NFM), (**b**). NFM-Al 1 wt.%, (**c**). NFM- 3 wt.%, and (**d**) to (**f**). The spreading behavior of water drop on the surface of NFM-Al 5 wt.% during 9 s of the test

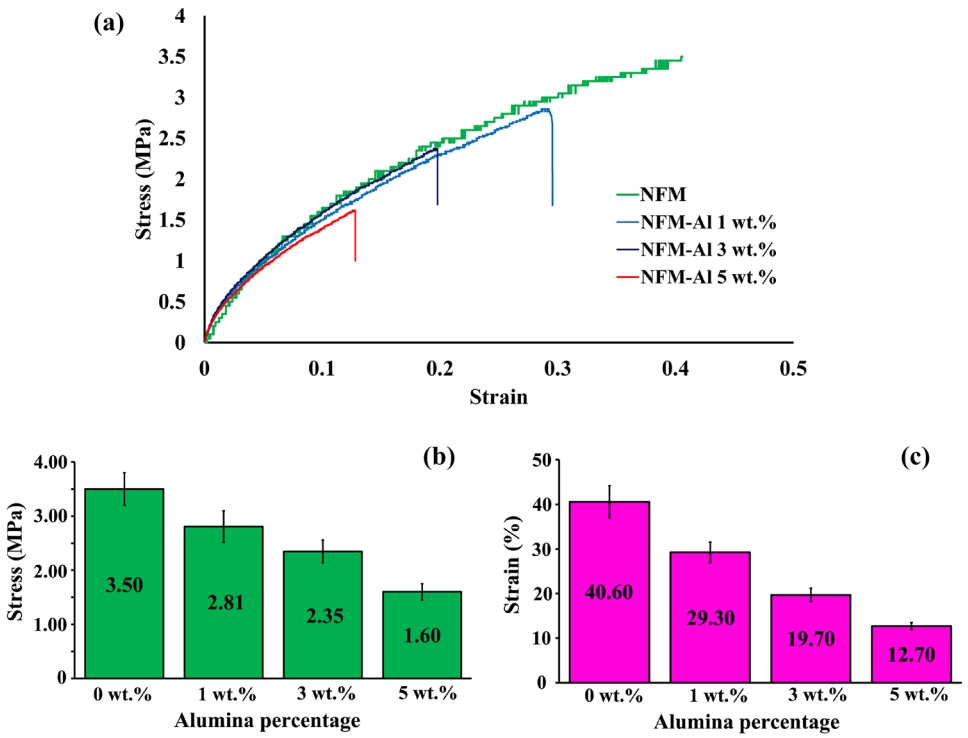

Fig. 7 (**a**). The stress-strain curves of ENCMs at different incorporation contents of the γ-alumina NPs, (**b**) and (**c**). The average values of the tensile strength and strain of ENCMs, respectively

significantly decreased from 2.81 to 1.60 MPa and 29.30 to 12.70 % by an increase in alumina content from 1 to 5 wt.%, respectively. According to Fig. 4, the γ-alumina NPs agglomerated at some sections of the nanofibers. The aggregated spots of the γ-alumina NPs can create defect-like structures in the fibers. These cluster-like structures can weaken the mechanical performance of the nanocomposite membranes by making the local stress concentration regions in the fibers, which in turn deteriorates the mechanical properties of ENCMs [64]. Different studies also proved that the addition of higher contents of nanoparticles can cause a significant drop in the mechanical properties of ENCMs, due to the agglomeration of the NPs and restriction of interface area [73, 81, 83, 84].

The tensile strength of the membranes is a determining factor for their working pressure [85]. The MF membranes usually work under low trans-membrane pressure conditions (0.1-2 bar, 0.2 MPa) [86–88]. However, the electrospun membranes were tested under 0.8 MPa pressure for pure water test and no damage or burst was observed under the enhanced condition. On the other hand, it should be noted that the tensile strength of the membranes was measured without the common supporting layer that is used in the industry to provide mechanical support for thin-layer membranes [85, 89]. Considering the operating pressure of ENCMs (0.2 bar, 2 MPa) the threshold of 2 MPa for tensile strength could be enough for the microfiltration process, which was covered by NFM-Al 1 wt.% and NFM-Al 3 wt.% membranes.

Filtration efficiency of ENCMs

Figure 8a shows the permeation flux of nanocomposite nanofiber membranes. Results showed higher permeation flux for NFM-Al 5 wt.% membrane (about 102 $L.m^2.h^{-1}$). The higher membrane flux at the first step of filtration could be related to higher total porosity (90.3 %) and hydrophilicity (WCA = 27.3°) of the γ-alumina incorporated ENCMs. Figure 8a shows an evident trend for the permeation flux of tested membranes. The initial and the final flux of ENCMs were increased by incorporation and increase in the content of the γ-alumina NPs. The initial and the final permeation flux of nanocomposite membranes were increased from 49 to 102 $L.m^2.h^{-1}$ and from 16.4 to 27.7 $L.m^2.h^{-1}$, respectively. The results could be explained by an improvement in the hydrophilic features of ENCMs with the increase in the alumina content from 0 to 5 wt.% and the increase in the total porosity of ENCMs from 70.2 to 90.3 %. The hydrophilicity of nanocomposite membranes increase due to the presence of hydrophilic hydroxyl groups in the γ-alumina NPs, which in turn could be resulted in a decrease in the affinity of HA molecules to absorb to the surface of ENCMs [50].

The calculated parameters, including IFR, RFR, FRR and TFR, were used to study the fouling behavior of ENCMs. The calculated parameters are listed in Table 4. Although reversible fouling could be recovered by physical cleaning, irreversible fouling results from the entrapment of the foulant particles inside the internal pores or adsorption of the pollutants on the surface of membranes

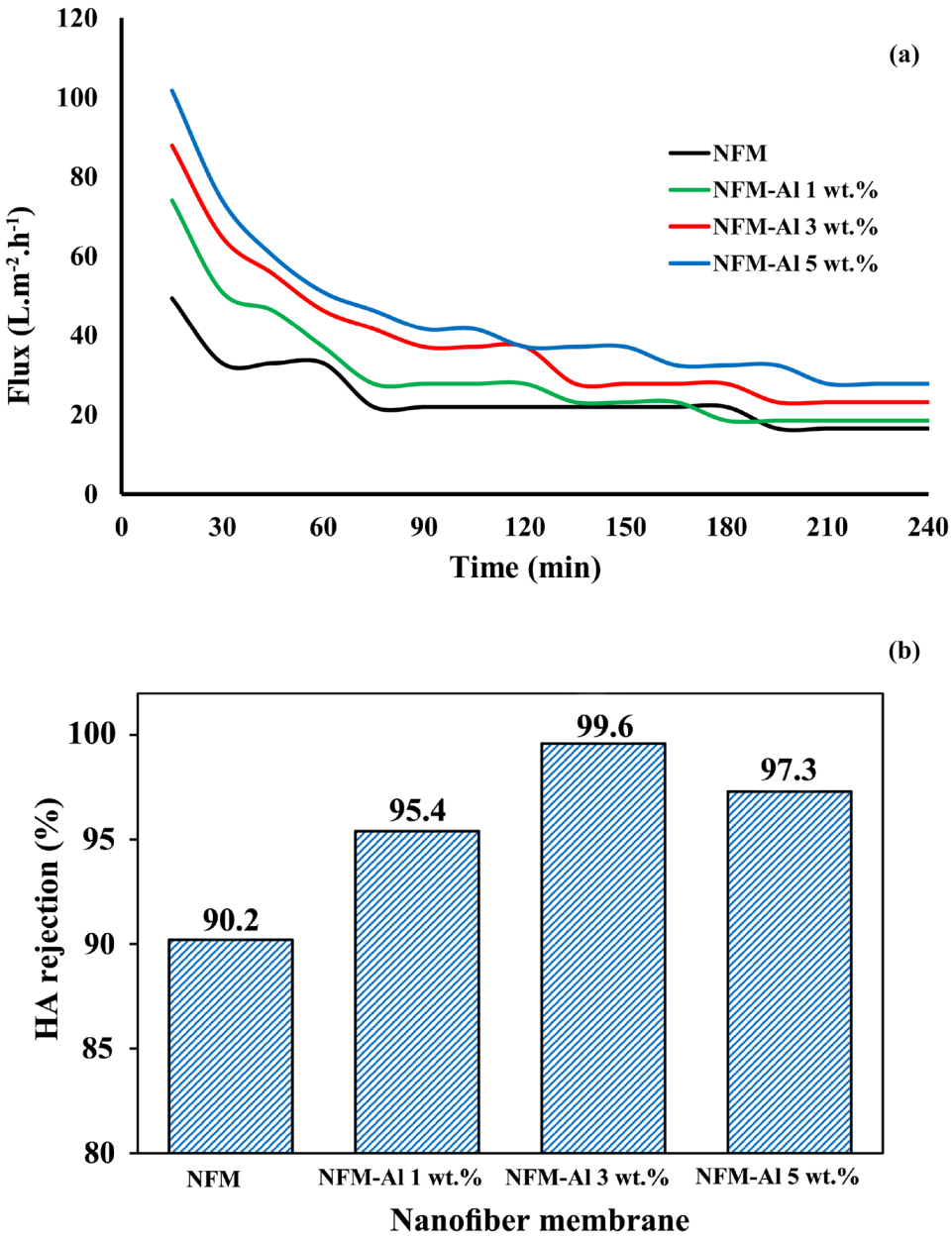

Fig. 8 Results of the filtration test for ENCMs at different contents of the γ-alumina NPs (TMP = 0.2 bar): (**a**). Permeation flux and (**b**). The pollutant rejection efficiency of ENCMs

[90]. The irreversible fouling can increases the process complexity and reduces the working life of the membranes [91]. Results showed a decrease in IFR value from 11.1% to 5.6% by an increase in content of the γ-alumina NPs from 0 to 3 wt.%. However, the irreversible fouling ratio of the nanocomposite membranes increased slightly (from 5.6% to 5.9%) by increase in the content of the γ-alumina NPs from 3 to 5 wt.%. This result could be attributed to the non-uniform structure of the nanofibers with the increase of the γ-alumina NPs up to 5 wt.% (see Fig. 3d). The surface morphology of NFM-Al 5 wt.% membrane consists of non-fibrous smooth sites, so the pollutants entrapped within the interconnected pore structures cannot be washed away. Thus, the irreversible fouling parameter of the membrane was increased slightly than NFM-Al 3 wt.% sample. The current results for enhancement in the anti-fouling properties and permeation flux by using γ-alumina NPs were also in agreement with the literature [49, 50].

Table 4 Fouling parameters of ENCMs (TMP = 0.2 bar)

Membrane	Alumina content (% w/w)	RFR (%)	IFR (%)	FRR (%)	TFR (%)
NFM	0	81.5	11.1	88.9	92.6
NFM-Al 1 wt.%	1	91.8	6.7	93.3	98.5
NFM-Al 3 wt.%	3	92.6	5.6	94.4	98.2
NFM-Al 5 wt.%	5	92.0	5.9	94.1	97.9

The anti-fouling property could be affected porosity and hydrophilicity of the membranes [92]. Upon further addition of the γ-alumina NPs into membranes, the hydrophilicity and porosity of ENCMs were improved significantly (see Table 3 and Fig. 6). The decrease in IFR of ENCMs is ascribed to the improvement in the porosity and hydrophilicity of ENCMs [93]. The hydrophilicity of the membranes causes the formation of a layer of water on the surface of ENCMs [75]. Consequently, hydrophobic molecules of the humic acid cannot be attached to the membrane surface, which resulting in to a decrease in IFR value. Furthermore, the anti-fouling performance of the membranes could also be explained based on the surface electrostatic interactions (zeta potential of the membrane surface). Breite et al. proved the zeta potential effects on anti-fouling properties of the membranes [94]. Ghezelgheshlaghi et al. reported the decrease in the zeta potential of the PAN membrane incorporated with alumina NPs [95]. Considering the negative charge of most soluble pollutants (including humic acid), the decrease in the positive charge of the membranes enhances the anti-fouling feature of ENCMs [96–98]. Incorporation of the γ-alumina NPs into membranes may be resulted in to reduction of the zeta potential of ENCMs, resulting in to decrease in the positive charge of the surface of the membranes. As a result, the affinity of the negatively charged pollutants (like humic acid) to stick to the surface of the membranes will be reduced, leading to improving the anti-fouling properties of ENCMs.

The reversible fouling ratio of ENCMs was also measured according to Equation (5). RFR parameter represents the portion of total fouling that could be recovered by physical cleaning. Results showed that RFR parameter of the γ-alumina loaded ENCMs increased from 81.5 to 92.6% with incorporation and increase in the content of γ-alumina NPs from 0 to 3 wt.%. The increase in RFR value improved the reusability of the nanocomposite structures compared to neat PVC/TPU/PC membranes. Although, RFR of NFM-Al 5 wt.% sample decreased slightly from 92.6 to 92.0% by an increase in the content of NPs, the reversible fouling of the membrane was higher than the neat PVC/TPU/PC (NFM) and NFM-Al 1 wt.% membranes. The increase in RFR value of ENCMs by incorporation of the γ-alumina NPs is in agreement with the literatures. Etemadi et al. reported the improvement in the RFR parameter of the PVC membranes by incorporating 2 wt.% alumina from 28.6 to 32.7 % [73]. It has also been reported that the alumina NPs could be affected the reversible fouling of PVC-PU membranes [50]. The enhancement in the RFR parameter of ENCMs could be explained by the hydrophilicity of the γ-alumina NPs, which prevents the adsorption of organic pollutants on the surface of membranes [75].

Membranes with higher FRR values exhibit better anti-fouling behavior [73, 82]. As presented in Table 4, the NFM-Al 3 wt.% membrane also had a higher FRR value (94.4%), which is in agreement with its lower irreversible fouling ratio. Incorporation and increase in the contents of the γ-alumina NPs from 1 to 3 wt.% in ENCMs led to increase in FRR of the membranes from 88.9% to 94.4%. Although the hydrophilicity of membranes had a critical effect on the fouling properties of the membranes, the surface morphology and uniformity of nanofiber structures affected the anti-fouling characteristics of ENCMs. Thus, the 3 wt.% of the alumina content could be considered an optimum level for incorporation of the alumina NPs in membranes.

TFR represents the sum of reversible and irreversible fouling. Results showed that TFR parameter of ENCMs increased by incorporation of the γ-alumina NPs from 92.6 to 98.5%. However, TFR value decreased with increase in the content of the γ-alumina NPs from 98.5 to 97.9%. Although, TFR of ENCMs was higher than the neat structure, the higher portion of the total fouling belonged to reversible fouling (RFR), indicating the better anti-fouling performance of the electrospun membranes loaded by γ-alumina NPs [99].

The HA rejection of ENCMs

The UV visible spectroscopy was used to measure HA rejection level of the alumina-loaded ENCMs. The results for the removal of the humic acid are presented in Fig. 8b. According to Fig. 8b, NFM-Al 3 wt.% membrane exhibited the higher performance of HA rejection by removal of 99.6% of humic acid in filtered water. Results indicated that the incorporation of the γ-alumina NPs in PVC/TPU/PC membranes led to an improvement in the pollutant rejection of ENCMs compared with the neat nanofibers. HA removal of ENCMs was increased from 90.2% up to 99.6% with the increase in the content of the γ-alumina NPs from 0 to 3 wt.%. However, HA removal of nanofiber composite was decreased from 99.6% to 97.3% by increase in the content of the γ-alumina NPs from 3 to 5 wt.%. This trend in agreement with the results of permeation flux could also be explained by morphology and non-uniformity of the nanofibers in NFM-Al 5 wt.% sample (see Fig. 3d). The increase of HA rejection by incorporation of the γ-alumina NPs could also be explained by improvement in the hydrophilicity of ENCMs. The hydrophilic nature of the membranes minimizes the interaction and tendency between foulant molecules and the surface of ENCMs. Accordingly, the possibility of forming a layer of water molecules on the surface of ENCMs is reduced, preventing from adsorption of the pollutants to the surface of membranes [50, 100].

Figure 9 shows the performance of the electrospun nanocomposite membranes for HA rejection during the filtration experiment. Figure 9a, b demonstrate the nanofiber membrane at the beginning and the end of the filtration test,

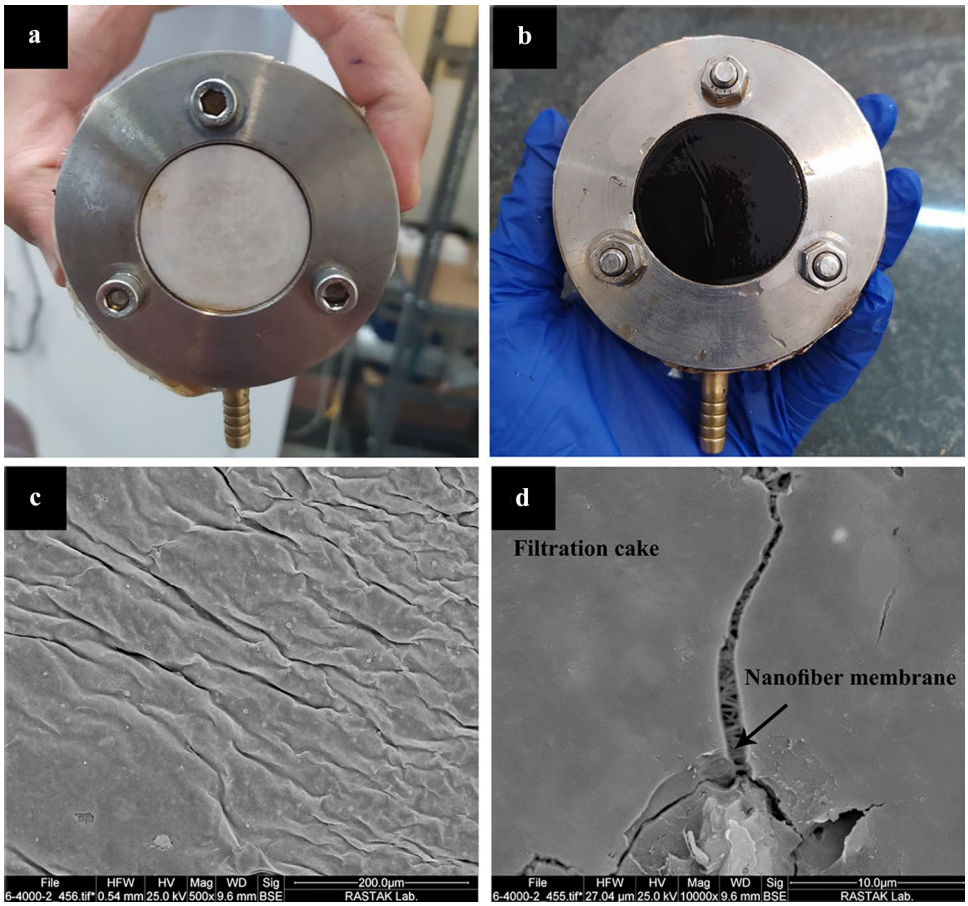

Fig. 9 (**a**), (**b**). The electrospun nanofiber nanocomposite membrane at the beginning and end of the test, respectively, (**c**) and (**d**). SEM images for filtration performance of the γ-alumina incorporated ENCM (NFM Al- 3 wt.%) at the different magnifications: 500X and 10000 X, respectively

respectively. Figure 9c, d show the SEM images of the filtration cake deposited on the surface of ENCM. SEM image in Fig. 9d clearly shows the boundary between the deposited layer and the nanofibers. HA rejection tests also revealed the better performance of NFM-Al 3 wt.% membrane compared with other samples.

Conclusion

In this paper, the blended nanofibers were produced at different content of the γ-alumina NPs (0, 1, 3 and 5 wt.%). SEM results showed that the diameter of ENCMs was in the range of 155-491 nm. Results revealed that the hydrophilicity of ENCMs was improved by an increase in the content of the γ-alumina from 0 to 5 wt.% (with the decrease in WCA from 80.3° to 27.3°). Mechanical tests showed a significant drop in mechanical properties due to the role of aggregated NPs as local stress concentration regions along the nanofibers (evidenced by EDS results). However, the mechanical parameters of the membranes remained within a reasonable range. The filtration tests using the submerged module (TMP = 0.2 bar), indicated the significant effects of the hydrophilicity and porosity of ENCMs on the rejection efficiency of the organic pollutants from the contaminated water. Filtration tests showed a higher fouling recovery ratio (FRR) of 94.4% for the NFM-Al 3 wt.% membrane. The irreversible fouling ratio of ENCMs also showed a decrease up to 5.6% by an increase in the content of the γ-alumina NPs from 0 to 5 wt.%. The pollutant (humic acid) rejection of ENCMs was raised (up to 99.6 %) with the increase in content of the γ-alumina NPs due to enhancement of the hydrophilicity of ENCMs that would minimize the interaction between foulant molecules and the surface of the nanofibers. The results, thus, revealed that incorporating the γ-alumina NPs up to 3 wt.% resulted in the enhanced anti-fouling properties of the electrospun nanocomposite nanofibers. However, NFM-Al 5 wt.% membrane also can be considered a desirable structure, if the hydrophilicity, porosity and permeation flux are intended for special application.

Supplementary Information The online version contains supplementary material available at https://doi.org/10.1007/s10965-023-03672-z.

Data availability The data that support the findings of this study are available on request from the corresponding author.

Declarations

Conflict of interest The authors declare that they have no known competing financial interests or personal relationships which could influence the work reported in this paper.

References

1. Tramblay Y, Koutroulis A, Samaniego L et al (2020) Challenges for drought assessment in the Mediterranean region under future climate scenarios. Earth Sci Rev 210:103348. https://doi.org/10.1016/j.earscirev.2020.103348
2. Sconiers WB, Rowland DL, Eubanks MD (2020) Pulsed drought: the effects of varying water stress on plant physiology and predicting herbivore response. Crop Sci 60:2543–2561. https://doi.org/10.1002/csc2.20235
3. Tortajada C (2020) Contributions of recycled wastewater to clean water and sanitation Sustainable Development Goals. npj Clean Water 3:22. https://doi.org/10.1038/s41545-020-0069-3
4. Drechsel P, Qadir M, Baumann J (2022) Water reuse to free up freshwater for higher-value use and increase climate resilience and water productivity. Irrig Drain 71:100–109. https://doi.org/10.1002/ird.2694
5. Ariaeenejad S, Motamedi E, Hosseini Salekdeh G (2021) Application of the immobilized enzyme on magnetic graphene oxide nano-carrier as a versatile bi-functional tool for efficient removal of dye from water. Bioresour Technol 319:124228. https://doi.org/10.1016/j.biortech.2020.124228
6. Yu S, Tang H, Zhang D, Wang S, Gang MQ, Song D, Fu, Baowei Hu XW (2021) MXenes as emerging nanomaterials in water purification and environmental remediation. Sci Total Environ 811:152280. https://doi.org/10.1016/j.scitotenv.2021.152280
7. Saffari R, Shariatinia Z, Jourshabani M (2020) Synthesis and photocatalytic degradation activities of phosphorus containing ZnO microparticles under visible light irradiation for water treatment applications. Environ Pollut 259:113902. https://doi.org/10.1016/j.envpol.2019.113902
8. Worch E (2021) Adsorption Technology in Water Treatment. De Gruyter, Dresden
9. Cui H, Huang X, Yu Z et al (2020) Application progress of enhanced coagulation in water treatment. RSC Adv 10:20231–20244. https://doi.org/10.1039/d0ra02979c
10. Pompa-Monroy DA, Iglesias AL, Dastager SG et al (2022) Comparative study of polycaprolactone electrospun fibers and casting films enriched with carbon and nitrogen sources and their potential use in water bioremediation. Membr (Basel) 12:327. https://doi.org/10.3390/membranes12030327
11. Işık C, Saraç N, Teke M, Uğur A (2021) A new bioremediation method for removal of wastewater containing oils with high oleic acid composition:Acinetobacter haemolyticuslipase immobilized on eggshell membrane with improved stabilities. New J Chem 45:1984–1992. https://doi.org/10.1039/d0nj05175f
12. Dehghani Y, Honarvar B, Azdarpour A, Nabipour M (2021) Treatment of wastewater by a combined technique of adsorption, electrocoagulation followed by membrane separation. Adv Environ Technol 7:171–183. https://doi.org/10.22104/AET.2021.5133.1394
13. Oliveira GA, Machado ÊL, Knoll RS et al (2022) Combined system for wastewater treatment: ozonization and coagulation via tannin-based agent for harvesting microalgae by dissolved air flotation. Environ Technol (United Kingdom) 43:1370–1380. https://doi.org/10.1080/09593330.2020.1830181
14. Ezugbe EO, Rathilal S (2020) Membrane technologies in wastewater treatment: a review. Membr (Basel) 10:89. https://doi.org/10.3390/membranes10050089
15. Reddy VS, Tian Y, Zhang C et al (2021) A review on electrospun nanofibers based advanced applications: from health care to energy devices. Polym (Basel) 13:3746. https://doi.org/10.3390/polym13213746
16. HMTShirazi R, Mohammadi T, Asadi AA, Tofighy MA (2022) Electrospun nanofiber affinity membranes for water treatment applications: a review. J Water Process Eng 47:102795. https://doi.org/10.1016/j.jwpe.2022.102795
17. Pervez MN, Mishu MR, Talukder ME et al (2022) Electrospun nanofiber membranes for the control of micro/nanoplastics in the environment. Water Emerg Contam Nanoplastics 1:10. https://doi.org/10.20517/wecn.2022.05
18. Su Y, Fan T, Cui W et al (2022) Advanced electrospun nanofibrous materials for efficient oil/water separation. Adv Fiber Mater 4:938–958. https://doi.org/10.1007/s42765-022-00158-3
19. Hartati S, Zulfi A, Maulida PYD et al (2022) Synthesis of electrospun PAN/TiO_2/Ag nanofibers membrane as potential air filtration media with photocatalytic activity. ACS Omega 7:10516–10525. https://doi.org/10.1021/acsomega.2c00015
20. Li N, Wang W, Zhu L et al (2021) A novel electro-cleanable PAN-ZnO nanofiber membrane with superior water flux and electrocatalytic properties for organic pollutant degradation. Chem Eng J 421:127857. https://doi.org/10.1016/j.cej.2020.127857
21. Roche R, Yalcinkaya F (2019) Electrospun polyacrylonitrile nanofibrous membranes for point-of-use water and air cleaning. ChemistryOpen 8:97–103. https://doi.org/10.1002/open.201800267
22. Baby T, Jose TE, John CTA, Thomas R (2021) A facile approach for the preparation of polycarbonate nanofiber mat with filtration capability. Polym Bull 78:3363–3381. https://doi.org/10.1007/s00289-020-03266-5
23. Alarifi IM, Alharbi AR, Khan MN et al (2018) Water treatment using electrospun PVC / PVP nanofibers as filter medium. J Mater Sci Res 2:43–49. https://doi.org/10.18689/ijmsr-1000107
24. Khan WS, Khan NU, Janjua MM (2019) Wastewater treatment with PVC electrospun nanofibrous membrane. In: 2019 Advances in Science and Engineering Technology International Conferences (ASET). IEEE, Dubai, United Arab Emirates
25. Ghiasvand S, Rahmani A, Samadi M et al (2021) Application of polystyrene nanofibers filled with sawdust as separator pads for separation of oil spills. Process Saf Environ Prot 146:161–168. https://doi.org/10.1016/j.psep.2020.08.044
26. Sundaran SP, Reshmi CR, Sujith A (2018) Tailored design of polyurethane based fouling-tolerant nanofibrous membrane for water treatment. New J Chem 42:1958–1972. https://doi.org/10.1039/c7nj03997b
27. Jiříček T, Komárek M, Lederer T (2017) Polyurethane nanofiber membranes for waste water treatment by membrane distillation. J Nanotechnol 2017:7143055. https://doi.org/10.1155/2017/7143035
28. Hu X, Chen X, Giagnorio M et al (2022) Beaded electrospun polyvinylidene fluoride (PVDF) membranes for membrane distillation (MD). J Memb Sci 661:120850. https://doi.org/10.1016/j.memsci.2022.120850
29. Nie Y, Zhang S, He Y et al (2022) One-step modification of electrospun PVDF nanofiber membranes for effective separation of oil–water emulsion. New J Chem 46:4734–4745. https://doi.org/10.1039/d1nj05436h
30. Pervez MN, Talukder ME, Mishu MR et al (2022) One-step fabrication of novel polyethersulfone-based composite electrospun nanofiber membranes for food industry wastewater treatment. Membr (Basel) 12:413. https://doi.org/10.3390/membranes12040413
31. Nazemidashtarjandi S, Mousavi SA, Bastani D (2017) Preparation and characterization of polycarbonate/thermoplastic

polyurethane blend membranes for wastewater filtration. J Water Process Eng 16:170–182. https://doi.org/10.1016/J.JWPE.2017.01.004
32. Quoc Pham L, Uspenskaya MV, Olekhnovich RO, Olvera Bernal RA (2021) A review on electrospun PVC nanofibers: fabrication, properties, and application. Fibers 9:12. https://doi.org/10.3390/fib9020012
33. Yekrang J, Mohseni L, Etemadi H (2023) Water treatment using PVC/TPU/PC electrospun nanofiber membranes. Fibers Polym 24:907–920. https://doi.org/10.1007/s12221-023-00100-3
34. Ahmad T, Guria C (2022) Progress in the modification of polyvinyl chloride (PVC) membranes: a performance review for wastewater treatment. J Water Process Eng 45:102466. https://doi.org/10.1016/j.jwpe.2021.102466
35. Yong M, Zhang Y, Sun S, Liu W (2019) Properties of polyvinyl chloride (PVC) ultrafiltration membrane improved by lignin: hydrophilicity and anti-fouling. J Memb Sci 575:50–59. https://doi.org/10.1016/J.MEMSCI.2019.01.005
36. Behboudi A, Jafarzadeh Y, Yegani R (2017) Polyvinyl chloride/polycarbonate blend ultrafiltration membranes for water treatment. J Memb Sci 534:18–24. https://doi.org/10.1016/j.memsci.2017.04.011
37. Julien TCM, Subramanyam MD, Katakam HC et al (2019) Ultrasoft polycarbonate polyurethane nanofibers made by electrospinning: fabrication and characterization. Polym Eng Sci 59:838–845. https://doi.org/10.1002/pen.25021
38. Chen R, Zhang H, Wang M et al (2021) Thermoplastic polyurethane nanofiber membrane based air filters for efficient removal of ultrafine particulate matter $PM_{0.1}$. ACS Appl Nano Mater 4:182–189. https://doi.org/10.1021/acsanm.0c02484
39. Liang W, Xu Y, Li X et al (2019) Transparent polyurethane nanofiber air filter for high-efficiency $PM_{2.5}$ capture. Nanoscale Res Lett 14:361. https://doi.org/10.1186/s11671-019-3199-0
40. Chen H, Huang M, Liu Y et al (2020) Functionalized electrospun nanofiber membranes for water treatment: a review. Sci Total Environ 739:139944. https://doi.org/10.1016/j.scitotenv.2020.139944
41. Akther N, Phuntsho S, Chen Y et al (2019) Recent advances in nanomaterial-modified polyamide thin-film composite membranes for forward osmosis processes. J Memb Sci 584:20–45. https://doi.org/10.1016/j.memsci.2019.04.064
42. Huh JY, Lee J, Bukhari SZA et al (2020) Development of TiO_2-coated YSZ/silica nanofiber membranes with excellent photocatalytic degradation ability for water purification. Sci Rep 10:17811. https://doi.org/10.1038/s41598-020-74637-1
43. Marinho BA, de Souza SMAGU, de Souza AAU, Hotza D (2021) Electrospun TiO_2 nanofibers for water and wastewater treatment: a review. J Mater Sci 56:5428–5448. https://doi.org/10.1007/s10853-020-05610-6
44. Sun H, Feng J, Song Y et al (2022) Preparation of the carbonized zif – 8@PAN nanofiber membrane for cadmium ion adsorption. Polym (Basel) 14:2523. https://doi.org/10.3390/polym14132523
45. Zhang M, Ma W, Cui J et al (2020) Hydrothermal synthesized UV-resistance and transparent coating composited superoloephilic electrospun membrane for high efficiency oily wastewater treatment. J Hazard Mater 383:121152. https://doi.org/10.1016/j.jhazmat.2019.121152
46. Talukder ME, Pervez MN, Jianming W et al (2022) Ag nanoparticles immobilized sulfonated polyethersulfone/polyethersulfone electrospun nanofiber membrane for the removal of heavy metals. Sci Rep 12:5814. https://doi.org/10.1038/s41598-022-09802-9
47. Jang W, Yun J, Park Y et al (2020) Polyacrylonitrile nanofiber membrane modified with ag/go composite for water purification system. Polym (Basel) 12:2441. https://doi.org/10.3390/polym12112441
48. Deepa K, Arthanareeswaran G (2022) Influence of various shapes of alumina nanoparticle in integrated polysulfone membrane for separation of lignin from woody biomass and salt rejection. Environ Res 209:112820. https://doi.org/10.1016/j.envres.2022.112820
49. Targol Hashemi M, Reza Mehrnia SG (2022) Influence of alumina nanoparticles on the performance of polyacrylonitrile membranes in MBR. J Environ Heal Sci Eng 20:375–384. https://doi.org/10.1007/s40201-021-00784-w
50. Etemadi H, Afsharkia S, Zinatloo-Ajabshir S, Shokri E (2021) Effect of alumina nanoparticles on the anti-fouling properties of polycarbonate-polyurethane blend ultrafiltration membrane for water treatment. Polym Eng Sci 61:2364–2375. https://doi.org/10.1002/pen.25764
51. Amusa AA, Ahmad AL, Adewole JK (2020) Mechanism and compatibility of pretreated lignocellulosic biomass and polymeric mixed matrix membranes: a review. Membr (Basel) 10:370–398. https://doi.org/10.3390/membranes10120370
52. Xu J, Tazawa N, Kumagai S et al (2018) Simultaneous recovery of high-purity copper and polyvinyl chloride from thin electric cables by plasticizer extraction and ball milling. RSC Adv 8:6893–6903. https://doi.org/10.1039/c8ra00301g
53. Idris A, Man Z, Maulud AS, Khan MS (2017) Effects of phase separation behavior on morphology and performance of polycarbonate membranes. Membr (Basel) 7:21. https://doi.org/10.3390/membranes7020021
54. Gallu R, Méchin F, Dalmas F et al (2020) On the use of solubility parameters to investigate phase separation-morphology-mechanical behavior relationships of TPU. Polym (Guildf) 207. https://doi.org/10.1016/j.polymer.2020.122882
55. Amin NAAM, Mokhter MA, Salamun N et al (2023) Anti-fouling electrospun organic and inorganic nanofiber membranes for wastewater treatment. South Afr J Chem Eng 44:302–317. https://doi.org/10.1016/j.sajce.2023.02.002
56. Tang Y, Cai Z, Sun X et al (2022) Electrospun nanofiber-based membranes for water treatment. Polym 14:2004. https://doi.org/10.3390/polym14102004
57. Hulsey S, Absar S, Choi H (2017) Comparative study of polymer dissolution techniques for electrospinning. Procedia Manuf 10:652–661. https://doi.org/10.1016/j.promfg.2017.07.010
58. Fang B, Ning F, Hu S et al (2020) The effect of surfactants on hydrate particle agglomeration in liquid hydrocarbon continuous systems: a molecular dynamics simulation study. RSC Adv 10:31027–31038. https://doi.org/10.1039/d0ra04088f
59. Kang SP, Lee D, Lee JW (2020) Anti-agglomeration effects of biodegradable surfactants from natural sources on natural gas hydrate formation. Energies 13:1107. https://doi.org/10.3390/en13051107
60. Naullage PM, Bertolazzo AA, Molinero V (2019) How do surfactants control the agglomeration of clathrate hydrates? ACS Cent Sci 5:428–439. https://doi.org/10.1021/acscentsci.8b00755
61. Mamun A, Sabantina L, Klöcker M et al (2022) Electrospinning nanofiber mats with magnetite nanoparticles using various needle-based techniques. Polym (Basel) 14:533. https://doi.org/10.3390/polym14030533
62. Glaubitz C, Rothen-Rutishauser B, Lattuada M et al (2022) Designing the ultrasonic treatment of nanoparticle-dispersions via machine learning. Nanoscale 14:12940–12950. https://doi.org/10.1039/d2nr03240f
63. Pradhan S, Hedberg J, Blomberg E et al (2016) Effect of sonication on particle dispersion, administered dose and metal release of non-functionalized, non-inert metal nanoparticles. J Nanoparticle Res 18:285. https://doi.org/10.1007/s11051-016-3597-5
64. Karbowniczek JE, Ura DP, Stachewicz U (2022) Nanoparticles distribution and agglomeration analysis in electrospun fiber based composites for desired mechanical performance of poly(3-hydroxybuty-rate-co-3-hydroxyvalerate (PHBV) scaffolds with

hydroxyapatite (HA) and titanium dioxide (TiO_2) towards me. Compos Part B Eng 241:110011. https://doi.org/10.1016/j.compositesb.2022.110011
65. Shojaeiarani J, Bajwa D, Holt G (2020) Sonication amplitude and processing time influence the cellulose nanocrystals morphology and dispersion. Nanocomposites 6:41–46. https://doi.org/10.1080/20550324.2019.1710974
66. Sandhya M, Ramasamy D, Sudhakar K et al (2021) Ultrasonication an intensifying tool for preparation of stable nanofluids and study the time influence on distinct properties of graphene nanofluids – A systematic overview. Ultrason Sonochem 73:105479. https://doi.org/10.1016/j.ultsonch.2021.105479
67. Sharifi A, Khorasani SN, Borhani S, Neisiany RE (2018) Alumina reinforced nanofibers used for exceeding improvement in mechanical properties of the laminated carbon/epoxy composite. Theor Appl Fract Mech 96:193–201. https://doi.org/10.1016/j.tafmec.2018.05.001
68. Zdraveva E, Mijovic B, Govorcin Bajsic E, Grozdanic V (2018) The efficacy of electrospun polyurethane fibers with TiO_2 in a real time weathering condition. Text Res J 88:2445–2453. https://doi.org/10.1177/0040517517723025
69. Kumar R, Kumar M, Awasthi K (2016) Functionalized Pd-decorated and aligned MWCNTs in polycarbonate as a selective membrane for hydrogen separation. Int J Hydrogen Energy 41:23057–23066. https://doi.org/10.1016/j.ijhydene.2016.09.008
70. Atrak K, Ramazani A, Taghavi S (2018) Green synthesis of amorphous and gamma aluminum oxide nanoparticles by tragacanth gel and comparison of their photocatalytic activity for the degradation of organic dyes. J Mater Sci Mater Electron 29:8347–8353. https://doi.org/10.1007/s10854-018-8845-2
71. Zhu L, Sun C, Chen L et al (2017) Influences of NH_4F additive and calcination time on the morphological evolution of α-Al_2O_3 from a milled γ-Al_2O_3 precursor. Z für Naturforsch B 72:665–670
72. Gohari B, Abu-Zahra N (2018) Polyethersulfone membranes prepared with 3-aminopropyltriethoxysilane modified alumina nanoparticles for Cu(II) removal from water. ACS Omega 3:10154–10162. https://doi.org/10.1021/acsomega.8b01024
73. Etemadi H, Qazvini H (2021) Investigation of alumina nanoparticles role on the critical flux and performance of polyvinyl chloride membrane in a submerged membrane system for the removal of humic acid. Polym Bull 78:2645–2662. https://doi.org/10.1007/s00289-020-03234-z
74. Elumalai P, Parthipan P, Huang M et al (2021) Enhanced biodegradation of hydrophobic organic pollutants by the bacterial consortium: impact of enzymes and biosurfactants. Environ Pollut 289:117956. https://doi.org/10.1016/j.envpol.2021.117956
75. Ruan H, Li B, Ji J et al (2018) Preparation and characterization of an amphiphilic polyamide nanofiltration membrane with improved anti-fouling properties by two-step surface modification method. RSC Adv 8:13353–13363. https://doi.org/10.1039/c8ra00637g
76. Yuan XS, Liu W, Zhu WY, Zhu XX (2020) Enhancement in flux and anti-fouling properties of polyvinylidene fluoride/polycarbonate blend membranes for water environmental improvement. ACS Omega 5:30201–30209. https://doi.org/10.1021/acsomega.0c04656
77. Malczewska B, Lochyński P, Charazińska S et al (2023) Electrospun silica-polyacrylonitrile nanohybrids for water treatments. Membr (Basel) 13:72. https://doi.org/10.3390/membranes13010072
78. Wang Y, Górecki RP, Stamate E et al (2019) Preparation of super-hydrophilic polyphenylsulfone nanofiber membranes for water treatment. RSC Adv 9:278–286. https://doi.org/10.1039/C8RA06493H
79. Shakiba M, Nabavi SR, Emadi H, Faraji M (2021) Development of a superhydrophilic nanofiber membrane for oil/water emulsion separation via modification of polyacrylonitrile/polyaniline composite. Polym Adv Technol 32:1301–1316. https://doi.org/10.1002/pat.5178
80. Yalcinkaya F, Siekierka A, Bryjak M (2017) Preparation of fouling-resistant nanofibrous composite membranes for separation of oily wastewater. Polym (Basel) 9:679. https://doi.org/10.3390/polym9120679
81. Li YJ, Chen GE, Xie HY et al (2022) Increasing the hydrophilicity and anti-fouling properties of polyvinylidene fluoride membranes by doping novel nano-hybrid ZnO@ZIF-8 nanoparticles for 4-nitrophenol degradation. Polym Test 113:107613. https://doi.org/10.1016/j.polymertesting.2022.107613
82. Moradi G, Zinadini S (2020) A high flux graphene oxide nanoparticles embedded in PAN nanofiber microfiltration membrane for water treatment applications with improved anti-fouling performance. Iran Polym J (English Ed 29:827–840. https://doi.org/10.1007/s13726-020-00842-4
83. Sahu A, Dosi R, Kwiatkowski C et al (2023) Advanced polymeric nanocomposite membranes for water and wastewater treatment: a comprehensive review. Polym (Basel) 15:540. https://doi.org/10.3390/polym15030540
84. Ashraf MA, Peng W, Zare Y, Rhee KY (2018) Effects of size and aggregation/agglomeration of nanoparticles on the interfacial/interphase properties and tensile strength of polymer nanocomposites. Nanoscale Res Lett 13:214. https://doi.org/10.1186/s11671-018-2624-0
85. Charlton AJ, Lian B, Blandin G et al (2020) Impact of FO operating pressure and membrane tensile strength on draw-channel geometry and resulting hydrodynamics. Membr (Basel) 10:111. https://doi.org/10.3390/membranes10050111
86. Anoar Ali Khan SB (2021) Membrane-based hybrid processes for wastewater treatment. Elsevier
87. Pal P (2020) Membrane-based technologies for environmental pollution control. Membr Technol Environ Pollut Control 1–763. https://doi.org/10.1016/C2018-0-00072-9
88. Nayak SK, Dutta K, Gohil JM (2022) Advancement in polymer-based membranes for water remediation
89. Liu F, Wang L, Li D et al (2019) A review: the effect of the microporous support during interfacial polymerization on the morphology and performances of a thin film composite membrane for liquid purification. RSC Adv 9:35417–35428. https://doi.org/10.1039/c9ra07114h
90. Peng J, Su Y, Shi Q et al (2011) Protein fouling resistant membrane prepared by amphiphilic pegylated polyethersulfone. Bioresour Technol 102:2289–2295. https://doi.org/10.1016/j.biortech.2010.10.045
91. Peldszus S, Hallé C, Peiris RH et al (2011) Reversible and irreversible low-pressure membrane foulants in drinking water treatment: identification by principal component analysis of fluorescence EEM and mitigation by biofiltration pretreatment. Water Res 45:5161–5170. https://doi.org/10.1016/j.watres.2011.07.022
92. Vatanpour V, Madaeni SS, Moradian R et al (2012) Novel antibifouling nanofiltration polyethersulfone membrane fabricated from embedding TiO_2 coated multiwalled carbon nanotubes. Sep Purif Technol 90:69–82. https://doi.org/10.1016/j.seppur.2012.02.014
93. Mahmodi G, Ronte A, Dangwal S et al (2022) Improving anti-fouling property of alumina microfiltration membranes by using atomic layer deposition technique for produced water treatment. Desalination 523:115400. https://doi.org/10.1016/j.desal.2021.115400
94. Breite D, Went M, Prager A, Schulze A (2016) The critical zeta potential of polymer membranes: how electrolytes impact membrane fouling. RSC Adv 6:98180–98189. https://doi.org/10.1039/c6ra19239d
95. Ghezelgheshlaghi S, Mehrnia MR, Homayoonfal M, Montazer-Rahmati MM (2018) Al_2O_3/poly acrylonitrile nanocomposite

membrane: from engineering design of pores to efficient biological macromolecules separation. J Porous Mater 25:1161–1181. https://doi.org/10.1007/s10934-017-0527-6

96. Plisko TV, Bildyukevich AV, Burts KS et al (2020) Modification of polysulfone ultrafiltration membranes via addition of anionic polyelectrolyte based on acrylamide and sodium acrylate to the coagulation bath to improve anti-fouling performance in water treatment. Membr (Basel) 10:264. https://doi.org/10.3390/membranes10100264
97. Teow YH, Ooi BS, Ahmad AL (2017) Study on PVDF-TiO_2 mixed-matrix membrane behaviour towards humic acid adsorption. J Water Process Eng 15:99–106. https://doi.org/10.1016/j.jwpe.2016.04.005
98. Arif Z, Sethy NK, Kumari L et al (2019) Anti-fouling behaviour of PVDF/TiO_2 composite membrane: a quantitative and qualitative assessment. Iran Polym J (English Ed 28:301–312. https://doi.org/10.1007/s13726-019-00700-y
99. Etemadi H, Fonouni M, Yegani R (2020) Investigation of anti-fouling properties of polypropylene/TiO_2 nanocomposite membrane under different aeration rate in membrane bioreactor system. Biotechnol Rep 25:e00414. https://doi.org/10.1016/j.btre.2019.e00414
100. Rabiee H, Farahani MHDA, Vatanpour V (2014) Preparation and characterization of emulsion poly(vinyl chloride) (EPVC)/TiO2 nanocomposite ultrafiltration membrane. J Memb Sci 472:185–193. https://doi.org/10.1016/j.memsci.2014.08.051